# Characterization of a Modulated X-Ray Source for Ion Mobility Spectrometry

Tobias Reinecke, 1 Steven Kenyon, 2 Keith Gendreau, 2 Brian H. Clowers 1\*

<sup>1</sup>Department of Chemistry, Washington State University, Pullman, Washington 99164, United States

<sup>2</sup>National Aeronautics and Space Administration, Goddard Space Flight Center, Greenbelt, MD, United States

\*Corresponding Author: <u>brian.clowers@wsu.edu</u>

#### **Abstract**

As a highly deployed field instrument for the detection of narcotics, explosives, and chemical warfare agents, drift tube ion mobility spectrometry relies heavily upon the performance of the ionization source and mechanism of ion beam modulation. For this instrumental platform ion chemistry plays a critical role in the performance of the instrument from a sensitivity and selectivity perspective, however, a range of instrumental components also occupy pivotal roles. Most notably, the mechanism of ion modulation or ion gating is a primary contributor to peak width in a drift tube ion mobility experiment. Unfortunately, physical ion gates rarely perform perfectly and in addition to serving as physical impediments to ion transmission, their modulation also has undesirable field effects. Using a recently developed modulated, non-radioactive, X-ray source we detail the performance of an IMS system that is free of a gating structure and utilizes the pulsed nature of the modulated x-ray source (MXS) for both ion generation and initiation of the IMS experiment. After investigating the influence of pulse duration and spatial X-ray beam width on the analytical performance of the instrument, the possibility of using multiplexing with a shutterless system is explored. By increasing ion throughput, the observed multiplexing gain compared to a signal averaged spectrum approaches the theoretical maximum and illustrates the capability of the MXS-IMS system to realize significant signal to noise improvements.

Keywords: Ion Mobility Spectrometry; Non-radioactive Ionization Source; Multiplexing; Ion Gating; X-ray ionization

#### Introduction

By leveraging favorable ionization chemistries, atmospheric pressure ion mobility spectrometers (IMS) routinely detect trace gasses at the parts per trillion level, even for measurement times less than a second.[1] Consequently, commercial IMS instruments are widely employed for the detection of toxic industrial compounds, drugs of abuse, explosives, and chemical warfare agents.[2–5]. Furthermore, there is a substantial body of IMS literature exploring a wide array of alternative applications of IMS ranging from food quality assurance to rapid medical diagnostics.[6–10]

In a highly simplistic fashion the emergent property of gas-phase ion mobility is based upon the average velocity of an ion population in a neutral buffer gas under the influence of a weak electric field.[11-14] Additionally, provided accurate information regarding ion characteristics (e.g. molecular conformation and charge location) and system parameters, the mobility of an ion may be predicted with a reasonable degree of accuracy. However, the critical, and often underappreciated aspect of ion generation often dictates the type of ion observed during an ion mobility experiment. Not surprisingly, a wide variety of ionization sources are employed to target selective reactant ion chemistry (i.e. indirect ionization) or direct analyte ionization.[15] Soluble, polar, non-volatiles are commonly ionized using electrospray while other non-volatile species are probed using direct ionization approaches such as laser ablation.[16-18] Methods for ionizing gaseous analytes, however, often vary greatly depending upon the application. Traditionally, IMS employ radioactive sources, such as <sup>63</sup>Ni or <sup>3</sup>H to generate a low density plasma of reactant ions capable of transferring a charge to the target analyte in the gas-phase.[1, 19] While these sources do not require an external power source and are virtually maintenance free, facile transportation of such

systems may prove problematic along with disposal of IMS systems at the end of the useful lifetime. For the same reasons that radioactive sources serve an important role in field-portable instrumentation, it is worth mentioning that radioactive sources cannot be shut off which complicates compliant instrument maintenance. Due to the technical and regulatory aspects of radioactive sources there is a growing demand for the development of non-radioactive alternative ion sources. Common alternatives to radioactive ionization sources include ultraviolet photoionization,[20] corona discharge,[21] dielectric barrier discharge,[22, 23] micro-plasma,[24] and non-radioactive electron emitters,[25, 26] or X-ray ionization.[27–29] Though these ionization sources all find utility for a wide variety of analytes, not all of these sources are compatible with pulsed operation.

In addition to the types of reactant ions formed by various ionization sources, their compatibility with the type of experiment is another consideration. For example, when coupling an ion source with an IMS cell care must be taken to ensure its operation is compatible with the high voltage environment necessary to establish an electric field within the drift cell. Once an ion source is chosen, the critical aspect of ion gating must be addressed. In traditional IMS systems, ions are admitted into the drift region by an ion gate. Ion gates described in the literature include the commonly used Bradbury Nielsen gate and the Tyndall-Powell gate,[30–33] but the field-switching shutter[1, 34, 35] and the more recently published tri-state, three-grid shutter also serve to effectively admit ions into a drift cell.[36, 37] While the performance of the tri-state and field-switching shutters can minimize gate depletion these gating schemes are still physical structures within the drift cell. As a consequence, ion transmission is strongly dependent upon the physical grid structures and

the magnitude of the electric field used during ion injection.[35] With a goal of maximizing ion utilization efficiency there is merit in exploring IMS approaches that effectively eliminate the physical gating structure.

Recently, the concept of a shutterless IMS was presented by Xu et al.,[38] using a pulsed corona discharge and Cochems et al.[39] and Bunert et al.[40] that used a non-radioactive electron emitter. That work primarily focused on a fundamental investigation of the shutterless system (e.g. influence of electron penetration depth, electrical field settings and ionization time). Compared to the previous investigations that were limited to constantly emitting x-ray sources, the current x-ray source developed by Gendreau et al.[41] incorporates an innovative method of generating discrete x-ray pulses by amplifying electrons produced via the photoelectric effect followed by acceleration of the electron cascade into a target. To highlight its compatibility with the IMS experiment, the modulation of the x-rays is achieved by a standard 0-5 V TTL logic which modulates a UV LED (Source). As a consequence, only the TTL signal needs to be modulated which obviates the need for high voltage switching to achieve a pulsed x-ray system. By locating the X-ray beam path orthogonally to the IMS drift axis, a narrow spatial range of analytes is ionized per pulse. Because the physical ion gate has been removed from the system, the capacitive coupling from gate closing and opening events with the Faraday plate is eliminated. This reduction in electronic noise opens new possibilities for signal multiplexing, as pulse coupling into the detector limits the effective gains in multiplexing gain observed in standalone IMS systems.

# **Experimental**

To demonstrate the compatibility of the modulated x-ray source (MXS) with the IMS experiment, we detail the influence of x-ray pulse width and spatial width of the X-ray beam on the ion mobility spectrum in signal average mode. Subsequently, using 2,4-lutidine as an initial example, we highlight the capacity of the MXS-IMS system to realize signal to noise gains that approach the theoretical maximum multiplexing gain compared to the traditional signal averaging experiment. As a first generation prototype, this system demonstrates a high degree of promise given its relatively small size, adaptability, and demonstrated similarity with the reactant ions produced by traditional sources.

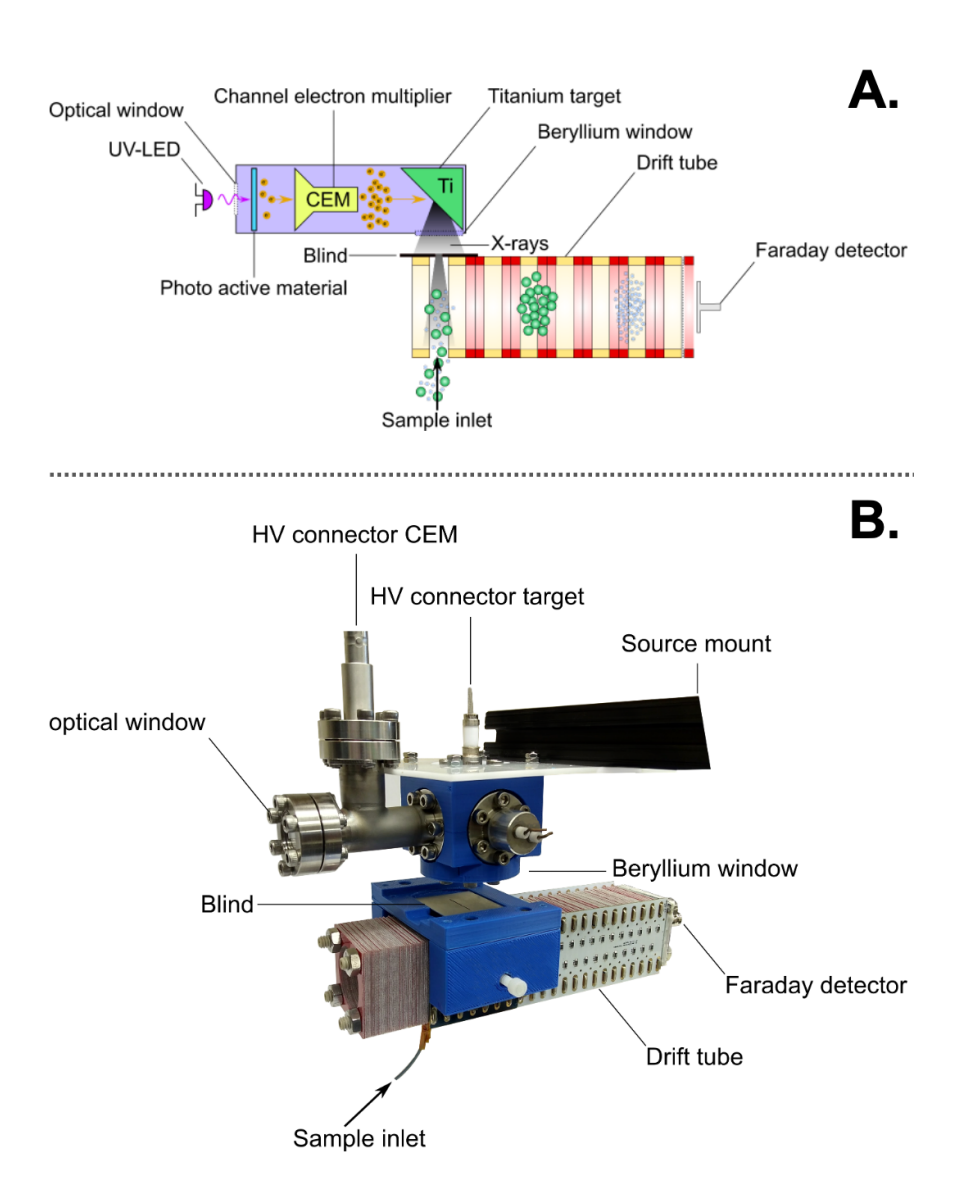


**Figure 1.** (A) Schematic of the IMS setup using the MXS ionization source. Pertinent features include the use of a modulated UV-LED to create an electron cascade within the channel electron multiplier (CEM). Electrons emitted from the CEM were accelerated into an angled titanium target to yield the pulsed X-ray beam for ionization. (B). Photo of the IMS setup including the MXS ionization source and blind holder for beam shaping.

**Instrumentation.** The drift tube used in this effort was constructed using printed circuit board manufacturing approaches described previously by Reinecke and Clowers.[42] A schematic of the MXS-IMS is depicted in **Figure 1A**. Based upon a stacked ring design with an optimized electrode aspect ratio, the drift cell is composed of electrodes with a nominal

ID of 25.4 mm and a spacing of 2 mm. Using this geometry, over 95% of the drift cell area is calculated to contain a homogeneous electric field.[43] The drift tube is terminated with a Faraday detector connected to a transimpedance amplifier (Keithley 427) operated with a gain of 109 and a 30 µs rise time. The total functional drift length (i.e. the distance from the center of the slit aperture to the Faraday detector) was 12.4 cm with electric fields ranging from ~400 to 550 V/cm. In a significant departure from traditional designs, the present configuration is not equipped with an ion gate to initiate the start of the experiment. Instead, the MXS is used to generate a user-defined pulse of X-rays which generates a spatially confined packet of ions within the IMS drift cell. The modulated x-ray source used in the present work was developed by Gendreau et al.[44] and is capable of yielding nanosecond wide pulses of x-rays characteristic of the target material. Compared to many x-ray sources that generate constant radiation, the current configuration is designed specifically to generate a well-defined pulse of x-rays and does not contain any active radioactive elements. To achieve this outcome a TTL-modulated UV LED emits UV photons that are transmitted through an optical window attached to an evacuated 1.33", 6-way ConFlat cube housing a modified channel electron multiplier (CEM) and target all held at a static ~10<sup>-7</sup> Torr in a sealed apparatus. Though not shown in **Figure 1**, a short length of ½" copper tube protrudes from one end of the ConFlat cube. This tube, which was used to pump down the MXS housing, was pinched closed and cut to realize the static vacuum needed for the CEM operation. Given the effectiveness of this seal the MXS does not require active pumping during operation. The total size of the MXS used in this effort was 14 cm x 10 cm x 10 cm and was constructed using off the shelf components.

To realize x-ray generation, photons from the pulse UV-LED, after passing through the UV window, are translated into electrons using a magnesium photocathode evaporated onto the entry changes of the CEM. Amplified electrons exciting the CEM are then accelerated into a titanium target with a user-defined potential (in this case 10.5 kV). Through this process an x-ray pulse mimicking the TTL pulse used to modulate the UV LED is translated into a packet of ionizing radiation that exits the evacuated housing through a 125 µm beryllium window in a beam oriented orthogonally to the axis of drift motion within the IMS cell. A key advantage of this x-ray source design worth restating is that the pulse of ionizing radiation is fully controlled by switching the 5 V power supply of the UV LED, which allows the creation of short but high intensity x-ray packets on a sub-µs time scale.

As x-rays have a comparably high penetration depth in air,[28, 29] the x-ray source was mounted in a way that any emitted beam penetrates the drift tube orthogonally to prevent the generation of ions in a large area inside the drift tube as shown by Bunert et al.[28, 29] To further decrease the area where ions are created and influence the spatial width of the generated ions, a holder to accommodate aluminum blinds with different slit widths was installed immediately below the beryllium window (See **Figure 1B**). These slits were milled out of 500 µm aluminum to have nominal slit widths that ranged from 0.5 mm to 1.5 mm and 20 mm long. For select experiments a set of micrometer-controller razor blades were used to incrementally adjust the slit width with ion currents being observed for slit widths down to 0.3 mm.

**Sample Introduction.** In a proof-of-principle application, gas-phase samples were introduced into the drift cell immediately after the entrance slit. Due to the counter-current flow of dried and sieve-purified drift gas (nitrogen at 690 Torr at 298 K) at ~500 mL/min neutral analytes were swept into the target beam path for ionization. Headspace from 2,4-lutidine was introduced via a gas-tight syringe (10 mL, SGE) through a 175 μm ID PEEK tube at a flow rate of 10 mL/hr (See the lower portion of **Figure 1B**.). Excess gas and unionized sample exited the system through an unrestricted aperture located at the entrance of the drift cell. Though the front of the apparatus in **Figure 1** was capped at the entrance a specific notch in a FR-4 spacer was made to allow for the exit of the drift gas and sample.

**Data Processing.** Modulation of the MXS using a TTL waveform and data acquisition was accomplished using the NIDAQ Tools module extension to IGOR Pro (Lake Oswego, OR) and a NI-6030E Multifunctional DAQ card. Pulsing sequences derived from Hadamard matrices were constructed using a modification to the polynomial construction method.[45] Specifically, the duty cycle of the target sequences was adjusted downward to maximize multiplier lifetime in a fashion similar to the approach presented previously by Clowers et al.[46] Additional details regarding this experimental modification to the pulsing sequences is presented in the subsequent sections.

### **Results and Discussion**

Comparison of generated ions from <sup>63</sup>Ni and the MXS. Prior to integrating the MXS with the IMS system, the pulsed source was coupled with an LTQ XL (Thermo Fisher Scientific, San Jose, CA) in an effort to characterize the range of reactant ions produced relative to a 10 mCi <sup>63</sup>Ni source. Though mobility was not the objective of initial source characterization,

the apparatus used (not shown) was effectively a shortened stack of electrodes placed in front of the LTQ XL inlet capillary. Because the stacked ring set could be biased relative to the capillary inlet, the time ions produced by the respective sources could reside at atmospheric pressure prior to entering the mass spectrometer and could similarly be adjusted. Figure 2 illustrates a representative range of spectra obtained with the standard <sup>63</sup>Ni source and the MXS in the negative and positive modes. Though small variations were observed between the peak intensities, the overall identities of the ions remained the constant between the two sources. These data illustrate the strong similarities between the sources in terms of their ion production characteristics. The spectra shown in the top row, Figure 2A and 2B, compare the <sup>63</sup>Ni and the corresponding MXS when the voltage applied to the 5 cm electrode stack was set to 500 V. Figure 2C and 2D illustrate the representative spectra acquired for the two ionization sources when the total potential across the electrode stack was set to 3 kV. All of the MXS data acquired in Figure 2 were obtained with a 10% pulsing duty cycle.

Interestingly, no significant differences were observed with respect to ion identities between the two sources suggesting that the ion chemistries available for use with MXS will mimic those known for <sup>63</sup>Ni. Given that the entrance to the stacked ring design attached to the ion trap was exposed to laboratory air, the observation of a wide variety of species in the positive mode was not entirely unexpected. It is worthy to note that the species observed in the positive mode correspond to many of the ions previously reported by Kumbhani et al. following a building floor treatment—an event that was also performed prior to the experiments shown in this effort.[47] In addition to the known clusters observed in the

positive mode, the species observed in the negative mode also conform to well-established ionization chemistries with nitrate as a terminal anion product. [48] An example of the nitrate anion chemistry is shown in **Figure S1** (Supporting Information). As the electric field strength is reduced the residence time of the ions prior to entering the mass analyzer is increased which enhances the concentration of the terminal, nitrate ion chemistry in air. [49, 50] **Figures 2B** and **2D** demonstrate the presence of the lactate anion, [51] which is not entirely unexpected given the 3D printed housing fabricated using polylactic acid (See **Figure 1B** and the blue CF cross housing). While subtle changes in ion intensity were observed between the two ionization sources, a high degree of similarities was observed suggesting that similar behavior would be expected for standard charge transfer and clustering reactions commonly employed in IMS used in security and screening applications.

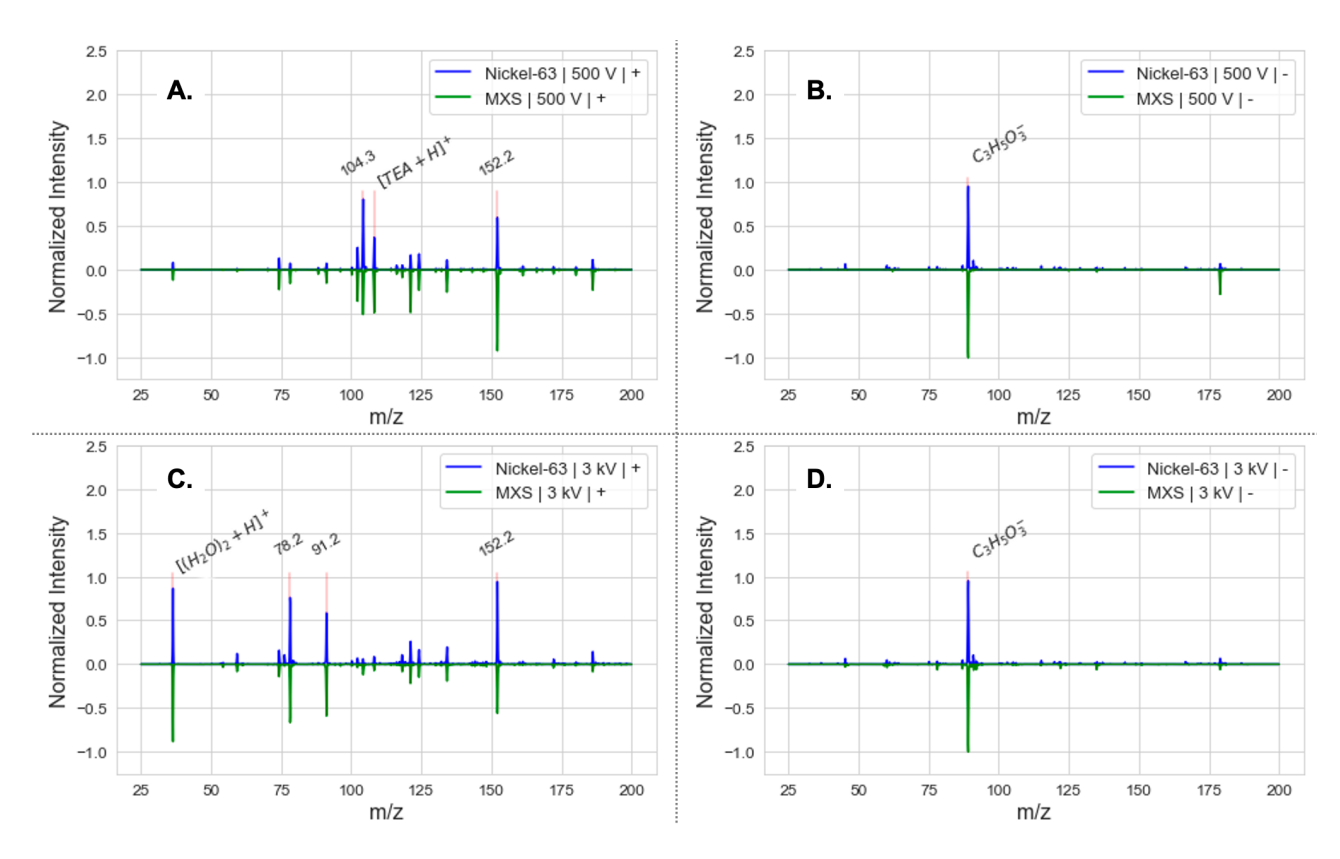


**Figure 2.** Comparing the ions produced by <sup>63</sup>Ni and the MXS system as measured at the inlet of the linear ion trap in both the positive and negative ion mode illustrates a high degree of similarity. For clarity, 2A and 2C correspond to the reactant ions produced in the positive mode for the radioactive and MXS system respectively. Plots 2B and 2D, demonstrate the ions produced in the negative mode by the two ion sources as slightly different acceleration voltages. Additional comparison regarding the raw intensities for the two ion sources and nitrate anion chemistry can be found in the Supportingl Information.

Single Pulse, Signal Averaged MXS-IMS. In a traditional single pulse, single averaged (SPSA) IMS experiment, a short packet of ions is injected into the drift region by altering the potential on an ion shutter for a short period of time relative to the entire mobility experiment. After traveling through the drift tube, the width of the ion packet at the detector is predominantly governed by the initial ion gate pulse width (GPW) and diffusion.[52] Contributions to the ion packet peak width is a function of the environmental parameters, the average drift time, t<sub>d</sub>, and, in the case of an orthogonal, pulsed ion source, the ionization time, t<sub>ion</sub>. Effectively an orthogonal, pulsed ionization source introduces a new spatial

contribution term that contributes to the observed peak width. In the present case, the effective spatial width of the ion packet is determined by the ionization time of MXS (scaled by the drift velocity), the spatial spread of the target analytes during ionization, and random diffusion. Similar to the considerations made by Bunert et al. for a pulsed electron emitter,[40] the temporal contribution of the spatial distribution of the ionizing radiation is determined by dividing the beam width by the velocity of the respective ion, L/t<sub>d</sub>. Consequently, the effective full width at half maximum (FWHM) for an ion population generated in the MXS source is summarized in Equation 1.

$$ext{FWHM} = \sqrt{\left[rac{16 \ln 2 \; k_{ ext{B}} \; T}{q \; V}
ight]^{rac{1}{2}} \; t_d + \left( ext{t}_{ ext{ion}} + rac{ ext{slit width} \cdot ext{t}_{ ext{d}}}{ ext{L}}
ight)^2}$$
 (1)

Here, k<sub>B</sub> is the Boltzmann constant, T is the absolute temperature, q is the elementary charge, V is the applied drift voltage, and L is the drift cell length. It is recognized that the assumptions in Equation 1 are a first approximation to the behavior observed in the MXS-IMS system.[29] Ideally, the temporal and spatial distributions would be mathematically convoluted to yield a more rigorous theoretical consideration of ion packet width. Recent work by Grabarics et al. introduces an extensive derivation of different peak models,[53] however, a key factor not accounted for is the potential for the spatial spreading of the X-rays passing through the slit. Though the width of the slit is considerable relative to the wavelength of the X-rays the MXS source itself is not a point source. This contribution to the spatial distribution of reactant ions is unknown and future efforts using orthogonal pulsed sources will focus on this behavior. Even though Equation 1 warrants continued evaluation, at a first approximation this relationship serves to effectively correct the shift in peak

centroids as a function of t<sub>ion</sub>. This correction will be discussed in the following sections and demonstrated graphically in **Figure S2**.

Despite the capacity to observe the expected R<sub>p</sub> gains, it is also worthy to note that the corrections to the arrival time distributions shown in Figure 3 and S2 do appear to conform to the second half of Equation 1. Specifically, the drift times for each spectrum were adjusted by a correction factor that accounts for the time of ionization and the salient feature of signal processing where the peak location is identified as the peak centroid while the physical timing of the data acquisition system occurs at t = 0. The factor used in this experimental case was determined by dividing the slit width by the velocity of the target analyte (e.g. **Equation 1**) and dividing this quantity again by half to correct for the difference between peak width and centroid location. In many ways, this correction procedure mirrors the standard practice of drift time correction used with physical ion grids commonly used in ion mobility spectrometry.[54, 55] It is recognized that this correction factor is an approximation as it relies upon the velocity of a specific species but the broad alignment of peak centroids further emphasizes the need to account for the spatiotemporal characteristics of the MXS. In an effort to evaluate this relationship, albeit somewhat qualitatively, the relationship in **Equation 1** were graphically evaluated with respect to the different factors expected to impact peak width (e.g. diffusion, tion, and drift velocity). After recognizing that as soon as an ion is created by the resulting reactant ions generated MXS pulse it begins migration, an evaluation of this contribution to the observed peak shape is considerable. In fact, for the limited range of slit widths on ionization times evaluated there is limited agreement with **Equation 1**. Future efforts that incorporate a spatially sensitive ion

detector could surely aid in answering the questions regarding the spatial spread of ions generated using a modulated x-ray source.

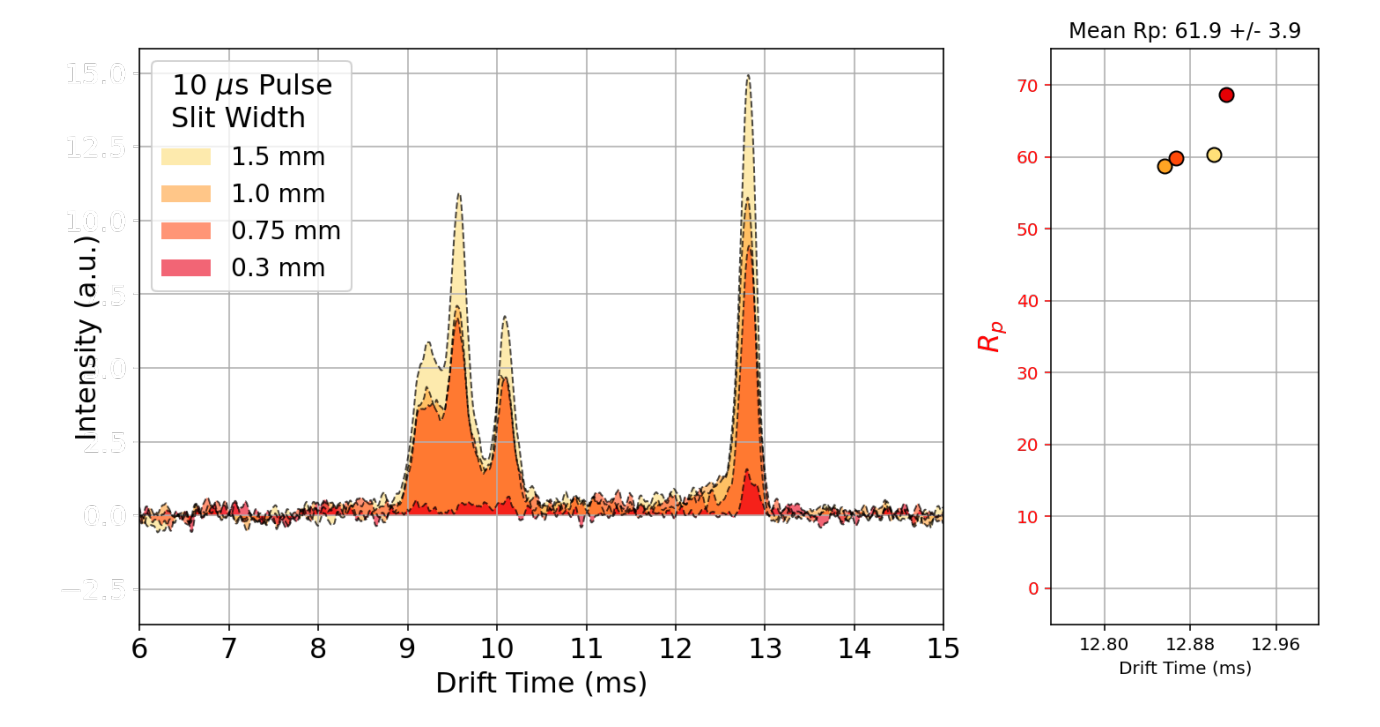


**Figure 3.** Representative ion mobility spectra acquired with the MXS at varying LED modulation duration periods and no physical ion gate using a 10 μs ionization time and varying slit widths. Drift times were corrected as a function of slit width and ion drift velocity. The correction procedure is outlined in **Figure S2**.

### **Hadamard Multiplexing**

Figures 3 and 5 show that resolving powers above 60 are achievable with the described experimental configuration. However, the experimental conditions leading to this result, specifically, a narrow x-ray slit and short ionization time, result in a reduced level of signal to noise ratio even after 1000 averages. As the MXS source was already operated at maximum target voltage and maximum CEM voltage, the only options to enhance the signal to noise ratio are either increasing the slit width or the ionization time. As expected from Equation 1, using wider slits would deteriorate the resolving power and is therefore not an ideal option. Thus, increasing the duty cycle of the ionization source by using Hadamard multiplexing is investigated in the following section. Instead of creating a single ion packet per scan, the ion source is pulsed in a pseudo-random fashion and the spectrum is obtained via circular correlation with the applied pulsing sequence. In this way, the signal to noise ratio is increased while maintaining the high resolving power of the system.

Generation of the simplex sequences used in this effort were based on the set of binary primitive polynomials and detailed in Appendix A.2 of Harwitt and Sloane.[45] The length of a pseudo random binary sequence (PRBS) derived from Hadamard matrices is well-defined, however, mapping any given sequence into the time-domain allows a degree of flexibility. At a minimum, the time length for any given Hadamard multiplexing experiment applied to IMS is directly related to the smallest time bin required for data analysis. For example, an 11-bit PRBS has a length of 2,047 elements (2<sup>11</sup>-1) and depending on the time resolution assigned to each element the necessary experiment length may be adjusted. During the standard construction Hadamard-derived simplex sequences (i.e. PRBS), the numbers of

ones and zeroes in the sequence is practically equal, leading to equal on and off time and thus a 50% duty cycle. However, in this particular case, in order to prevent overheating of the CEM inside the MXS, the duty cycle of the source was kept below 15%. To achieve this lower duty cycle, a modified simplex sequence was used. The approach to modifying the sequence with respect to duty cycle is described in detail by Clowers et al.[46]

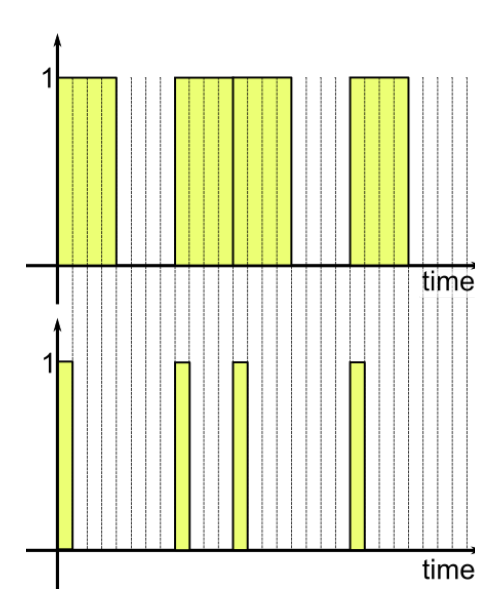


**Figure 4**. Schematic representation of the duty cycle reduction of a Hadamard pulsing sequence that established conditions where each ion gate pulse width is effectively the same. This latter point remains important to mitigate non-linear intensity variations with ionization time or ion injection widths.

To visualize the concept of duty cycle reduction of the Hadamard sequence an example sequence [1,0,1,1,0,1,0] is depicted in **Figure 4** (upper strace). In order to reduce the duty cycle from 50% to 12.5%, each element of the sequence is divided into 4 smaller bins. Subsequently, only the first sub bins are kept and the following 3 sub bins are set to zero, see **Figure 4** (lower trace). The original pulsing sequence contained 2047 elements and

when factoring in the sequence extension, the used modified sequence was comprised of  $(2^{11}\text{-}1)^*4\text{-}8188$  elements with each bin corresponding to 10 µs. Therefore, this sequence leads to a measured drift time spectrum with a length of  $8188^*10$  µs = 81.88 ms. The spectrum acquired with Hadamard multiplexing was averaged 250 times leading to an overall measurement time of 20.47 s. The length of the corresponding signal averaged mode spectra that were collected for comparison was set to  $0.25^*81.88 = 20.47$  ms. Therefore, the SGSA spectrum was averaged 1000 times in order to realize equal measurement times for the Hadamard multiplexing and signal averaged mode.[56]

$$m_{ideal} = Ax$$
 (4)

A is the cyclic matrix consisting of the pulsing sequence in the first row, which is subsequently circularly shifted by one bin to create each row below. For the estimation of the expected multiplexing gain, an error vector *e* is added, so that the multiplexed signal can be written as

$$m_{noisy}$$
= $Ax$ + $e$  (5)

For deconvolution, the multiplexed signal *m* is multiplied with the inverse of A, which is equal to performing a circular correlation as A is a cyclic matrix:

$$x_{HT} = A^{-1}m - A^{-1}e = A^{-1}m - n$$
 (6)

The noise  $n_i$  adding to each bin  $x_{HT,i}$  of the demultiplexed signal can be written as

$$n_i = \sum_i A^{-1}_{i,j} \mathbf{e}_j \tag{7}$$

Assuming a sufficiently long pulsing sequence and *e* being white Gaussian noise, equation 7 can be rewritten as

$$n_i = \sqrt{\sigma^2 \sum_j (Ai, j^{-1})^2}$$
 (8)

Here,  $\sigma$  is the standard deviation of e. Assuming that noise with the same standard deviation  $\sigma$  adds to a signal in signal average mode (i.e.  $x_{SA} = x + e$ ), the multiplexing gain for each bin in terms of noise reduction can be written as

$$G_i = 1/\sqrt{\sum_i (Ai, j^{-1})^2}$$
 (9)

To determine  $G_i$  for the modified HT sequence used in this work, eq. 9 was evaluated in Matlab. Interestingly we observed that  $G_i$  is equal for each bin (i.e. the noise is distributed equally over the demultiplexed spectrum). Furthermore, it appeared that  $G_i$  is equal to the multiplexing gain of the original pulsing sequence:

$$G_i = \sqrt{2^{11} - 1}/2 = 22.62$$

For additional details on the subtleties of pseudo random sequence creation, modification, and stretching, readers are directed to the review article by Reinecke et al.[57]. As stated before, the SA spectrum was averaged 1000 times and the HT spectrum for 250 times to account for the extended length of the HT sequence and realize equal acquisition times for better comparison. Therefore, the expected gain in the experiment is further reduced to

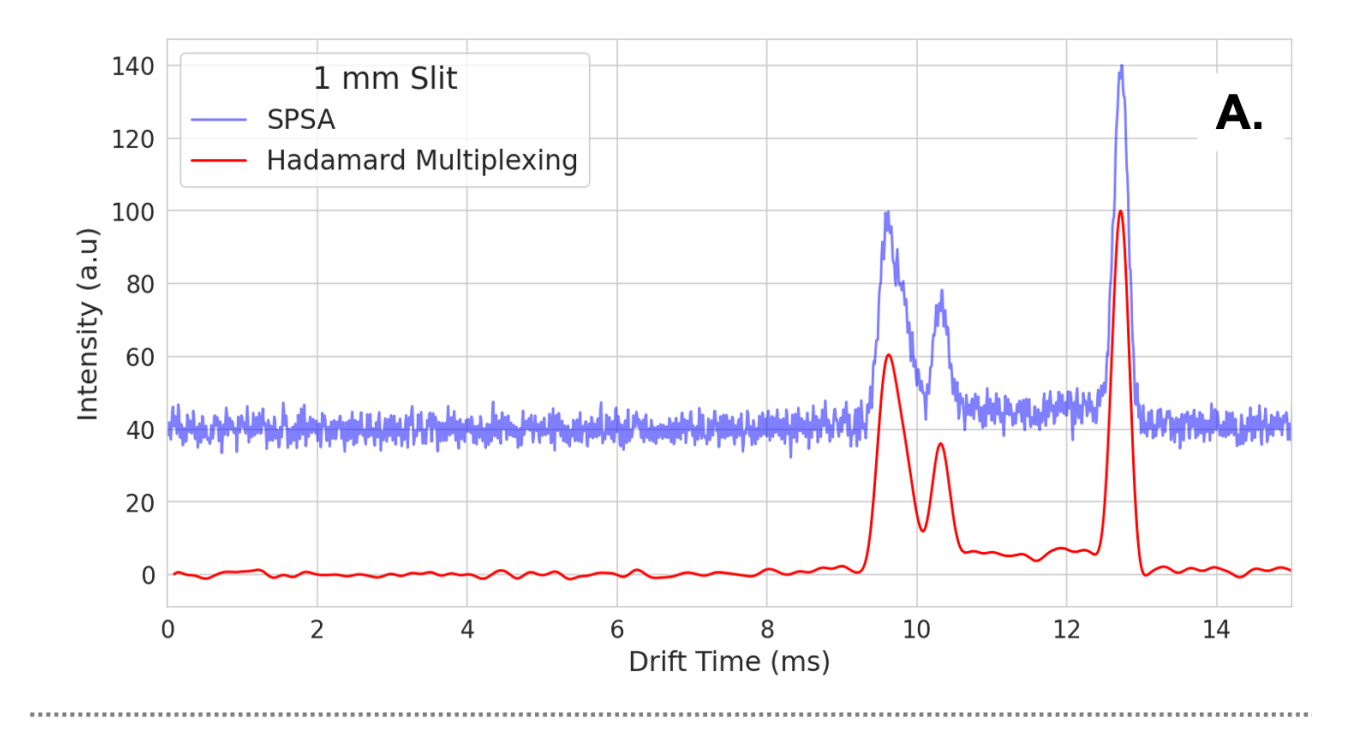
$$G_{experiment} = G_i \frac{\sqrt{250}}{\sqrt{1000}} = 0.5*22.62 = 11.31$$

In **Figure 5** spectra for 2,4-lutidine measured in SA-mode and HT-mode are compared. A statistical analysis of the noise in both spectra between 15 ms and 18 ms shows that HT-multiplexing reduces the standard deviation of the noise by a factor of  $\sigma$ SA/ $\sigma$ HT = 0.146/0.025 = 5.84. Because no physical gate is pulsed that can capacitively couple with

the Faraday plate, the noise contribution from that factor is effectively eliminated using the MXS system. While a detailed comparison between the MXS-IMS and a gated drift cell IMS is beyond the scope of this investigation, the capacitive coupling of the grid pulsing can be pronounced which drastically reduces the potential for the system to fully realize the multiplexing advantage. Clever experimental procedures (i.e. sequence inversion) and signal processing techniques can mitigate the impact of the gate ringing effect but they do not fully eliminate noise contributions.[58] **Figures S5-S7** present multiplexed data from an IMS of similar design to the MXS build that contains a physical ion gate. These plots illustrate the magnitude of the gate ringing that is often observed in a gridded system and its impact on signal recovery.

For the present gridless ion source, the elimination of the gate ringing drastically constrains the major contribution of noise compared to a traditional gridded IMS system. In such a scenario this reduction in detector noise for a multiplexing experiment allows the ultimate signal to noise ratio to align closer to the limits predicted by theory. The difference in the measured noise reduction in the MXS-IMS experiment compared to the noise reduction predicted by theory can be explained by the fact that only additive noise at the detector was considered in theory neglecting different other sources of noise like chemical noise or Fano noise that add to the ideal signal prior to multiplexing and cause lower measured gains than predicted. However, it is worthy to note that this result largely conforms to theory and when combined with the outlined rationale can be used as a benchmark for future comparison.[59] Readers are also directed towards an additional comparison of the multiplexed and single-pulse, signal averaged data shown in **Figure 5A** using a larger slit width (i.e 1.0 mm

compared to 0.3 mm in **Figure 5B**). Both slit widths illustrate the benefits afforded by multiplexing of the ion signal without the use of a physical ion gate with approximate multiplexing gains of 5.84 and 4.80 for **Figure 5A** and **5B**, respectively. Most importantly, these spectra highlight that without a physical ion shutter, capacitive coupling of the gate pulse (i.e. gate ringing) that would normally be observed (e.g. **Figure S5-S7**) is entirely absent when using the MXS.



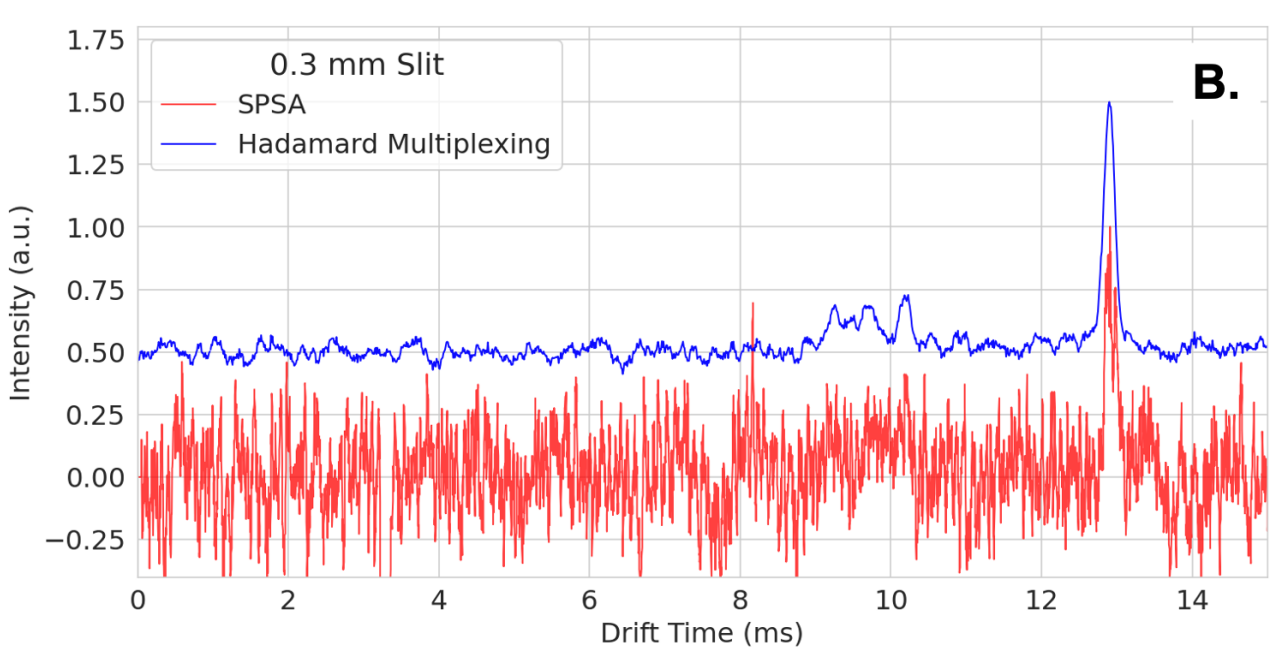


**Figure 5.** Direct comparison of the signal averaged versus the Hadamard multiplexing approach using 2,4-Lutidine. A. corresponds to a blind slit width of 1.0 mm and panel B represents the comparison for the 0.3 mm (i.e. razor blade slit). Because no physical gate is pulsed that can capacitively couple with the Faraday plate the noise contribution from this experimental factor is effectively eliminated using the MXS system. Compared to the plots shown in the Supporting Information using a gridded system, the gridless instrument here displays no gate ringing (as expected). The gain in SNR attributed to the multiplexing experiment for this spectrum is ~4.8.

## Conclusion

In this paper a compact, grounded, pulsed x-ray source was used as primary ionization source for gas-phase analytes measuring using an ion mobility spectrometer. Direct comparison of the ion species generated by the modulated x-ray source largely identical to those generated by the common beta emitter used in IMS (i.e. <sup>63</sup>Ni). This point is particularly salient, as the MXS represents an non-radioactive alternative ion source that provides direct access to the well-characterized ion chemistry of <sup>63</sup>Ni. Additionally, and perhaps, the most intriguing aspect of the MXS is the rapid discrete nature of the pulse x-ray beam and its use as an ion generation and gating mechanism for IMS. As previously noted by Bunert et al. the pulsed nature of the ionization source reduces the ion current generated which minimizes the SNR for a standard single pulse, signal averaging approach. It is for precisely these reasons that multiplexing is an ideal operational mode for a gridless IMS system. Following this approach, we demonstrate the capacity of this first-prototype to realize significant gains in signal-to-noise ratio when operating in a multiplexed configuration.

# **Acknowledgements**

Support was provided by NSF CHE-1506672 (TR and BHC) and NASA (SK and KG).

# **Associated Content**

Supporting Information. Additional plots detailing the performance of the multiplexing approach and theoretical performance of the system.

# **Author Information**

 $Corresponding \ author: \ ^*Brian \ Clowers; \ brian.clowers@wsu.edu$ 

ORCID:

Brian H. Clowers: 0000-0002-5809-9379

#### References

- 1. Kirk, A.T., Allers, M., Cochems, P., Langejuergen, J., Zimmermann, S.: A compact high resolution ion mobility spectrometer for fast trace gas analysis. Analyst. 138, 5200 (2013)
- 2. Ewing, R.G., Atkinson, D.A., Eiceman, G.A., Ewing, G.J.: A critical review of ion mobility spectrometry for the detection of explosives and explosive related compounds. Talanta. 54, 515–529 (2001)
- 3. Wu, C., Steiner, W.E., Tornatore, P.S., Matz, L.M., Siems, W.F., Atkinson, D.A., Hill, H.H., Jr: Construction and characterization of a high-flow, high-resolution ion mobility spectrometer for detection of explosives after personnel portal sampling. Talanta. 57, 123–134 (2002)
- Eiceman, G.A., Snyder, A.P., Blyth, D.A.: Monitoring of Airborne Organic Vapors Using Ion Mobility Spectrometry, http://dx.doi.org/10.1080/03067319008026945, (1990)
- 5. Kanu, A.B., Hill, H.H., Jr: Identity confirmation of drugs and explosives in ion mobility spectrometry using a secondary drift gas. Talanta. 73, 692–699 (2007)
- Vautz, W., Zimmermann, D., Hartmann, M., Baumbach, J.I., Nolte, J., Jung, J.: Ion mobility spectrometry for food quality and safety. Food Addit. Contam. 23, 1064–1073 (2006)
- 7. Jünger, M., Vautz, W., Kuhns, M., Hofmann, L., Ulbricht, S., Baumbach, J.I., Quintel, M., Perl, T.: Ion mobility spectrometry for microbial volatile organic compounds: a new identification tool for human pathogenic bacteria. Appl. Microbiol. Biotechnol. 93, 2603–2614 (2012)
- 8. Vautz, W., Baumbach, J.I., Westhoff, M., Züchner, K., Carstens, E.T.H., Perl, T.: Breath sampling control for medical application, http://dx.doi.org/10.1007/s12127-010-0039-4, (2010)
- Ruszkiewicz, D.M., Sanders, D., O'Brien, R., Hempel, F., Reed, M.J., Riepe, A.C., Bailie, K., Brodrick, E., Darnley, K., Ellerkmann, R., Mueller, O., Skarysz, A., Truss, M., Wortelmann, T., Yordanov, S., Thomas, C.L.P., Schaaf, B., Eddleston, M.: Diagnosis of COVID-19 by analysis of breath with gas chromatography-ion mobility spectrometry - a feasibility study. EClinicalMedicine. 100609 (2020)
- Baumbach, J.I., Sielemann, S., Xie, Z., Schmidt, H.: Detection of the Gasoline Components Methyltert-Butyl Ether, Benzene, Toluene, andm-Xylene Using Ion Mobility Spectrometers with a Radioactive and UV Ionization Source, http://dx.doi.org/10.1021/ac020342i, (2003)
- 11. Revercomb, H.E., Mason, E.A.: Theory of plasma chromatography/gaseous electrophoresis. review. Anal. Chem. 47, 970–983 (1975)
- 12. Kihara, T.: The Mathematical Theory of Electrical Discharges in Gases. Rev. Mod. Phys. 24, 45–61 (1952)
- 13. Kihara, T.: The Mathematical Theory of Electrical Discharges in Gases. B. Velocity-Distribution of Positive Ions in a Static Field. Rev. Mod. Phys. 25, 844–852 (1953)
- Siems, W.F., Viehland, L.A., Hill, H.H., Jr: Improved Momentum-Transfer Theory for Ion Mobility.
   Derivation of the Fundamental Equation. Anal. Chem. 84, 9782–9791 (2012)
- 15. Waraksa, E., Perycz, U., Namieśnik, J., Sillanpää, M., Dymerski, T., Wójtowicz, M.,

- Puton, J.: Dopants and gas modifiers in ion mobility spectrometry. Trends Analyt. Chem. 82, 237–249 (2016)
- Huang, S.D., Kolaitis, L., Lubman, D.M.: Detection of Explosives Using Laser Desorption in Ion Mobility Spectrometry/Mass Spectrometry, http://dx.doi.org/10.1366/0003702874447365, (1987)
- Ehlert, S., Walte, A., Zimmermann, R.: Ambient pressure laser desorption and laser-induced acoustic desorption ion mobility spectrometry detection of explosives. Anal. Chem. 85, 11047–11053 (2013)
- 18. Villatoro, J., Zühlke, M., Riebe, D., Riedel, J., Beitz, T., Löhmannsröben, H.-G.: IR-MALDI ion mobility spectrometry. Anal. Bioanal. Chem. 408, 6259–6268 (2016)
- 19. Crawford, C.L., Hill, H.H.: Comparison of reactant and analyte ions for <sup>63</sup>Nickel, corona discharge, and secondary electrospray ionization sources with ion mobility-mass spectrometry. Talanta. 107, 225–232 (2013)
- 20. Cheng, S., Wang, W., Zhou, Q., Chen, C., Peng, L., Hua, L., Li, Y., Hou, K., Li, H.: Fast Switching of CO3(-)(H2O)n and O2(-)(H2O)n reactant ions in dopant-assisted negative photoionization ion mobility spectrometry for explosives detection. Anal. Chem. 86, 2687–2693 (2014)
- 21. Borsdorf, H., Schelhorn, H., Flachowsky, J., Döring, H.-R., Stach, J.: Corona discharge ion mobility spectrometry of aliphatic and aromatic hydrocarbons, http://dx.doi.org/10.1016/s0003-2670(99)00567-x, (2000)
- 22. Olenici-Craciunescu, S.B., Michels, A., Meyer, C., Heming, R., Tombrink, S., Vautz, W., Franzke, J.: Characterization of a capillary dielectric barrier plasma jet for use as a soft ionization source by optical emission and ion mobility spectrometry, http://dx.doi.org/10.1016/j.sab.2009.10.001, (2009)
- 23. Jafari, M.T.: Low-temperature plasma ionization ion mobility spectrometry. Anal. Chem. 83, 797–803 (2011)
- 24. Vautz, W., Michels, A., Franzke, J.: Micro-plasma: a novel ionisation source for ion mobility spectrometry. Anal. Bioanal. Chem. 391, 2609–2615 (2008)
- 25. Heptner, A., Cochems, P., Langejuergen, J., Gunzer, F., Zimmermann, S.: Investigation of ion-ion-recombination at atmospheric pressure with a pulsed electron gun. Analyst. 137, 5105–5112 (2012)
- 26. Cochems, P., Runge, M., Zimmermann, S.: A current controlled miniaturized non-radioactive electron emitter for atmospheric pressure chemical ionization based on thermionic emission, http://dx.doi.org/10.1016/j.sna.2013.11.033, (2014)
- 27. Pershenkov, V.S., Tremasov, A.D., Belyakov, V.V., Razvalyaev, A.U., Mochkin, V.S.: X-ray ion mobility spectrometer, http://dx.doi.org/10.1016/j.microrel.2005.07.003, (2006)
- 28. Reinecke, T., Kirk, A.T., Heptner, A., Niebuhr, D., Böttger, S., Zimmermann, S.: A compact high-resolution X-ray ion mobility spectrometer. Rev. Sci. Instrum. 87, 053120 (2016)
- 29. Bunert, E., Reinecke, T., Kirk, A.T., Bohnhorst, A., Zimmermann, S.: Ion mobility spectrometer with orthogonal X-Ray source for increased sensitivity. Talanta. 185, 537–541 (2018)
- 30. Tyndall, A.M., Pearce, A.F.: The variation of the mobility of gaseous ions with temperature I--Positive ions in their own gas. Proceedings of the Royal Society of London. Series A-Mathematical and Physical Sciences. 149, 426–434 (1935)

- 31. Ni, K., Guo, J., Ou, G., Zhang, X., Yu, Q., Qian, X., Wang, X.: Study of ion transmission for a linear mode Bradbury–Nielsen gate in ion mobility spectrometer. Int. J. Mass Spectrom. 379, 75–79 (2015)
- 32. Clowers, B.H., Hill, H.H., Jr: Mass analysis of mobility-selected ion populations using dual gate, ion mobility, quadrupole ion trap mass spectrometry. Anal. Chem. 77, 5877–5885 (2005)
- 33. Bradbury, N.E., Nielsen, R.A.: Absolute Values of the Electron Mobility in Hydrogen. Phys. Rev. 49, 388–393 (1936)
- 34. Kirk, A.T., Zimmermann, S.: Bradbury-Nielsen vs. Field switching shutters for high resolution drift tube ion mobility spectrometers, http://dx.doi.org/10.1007/s12127-014-0153-9, (2014)
- 35. Kirk, A.T., Kueddelsmann, M.J., Bohnhorst, A., Lippmann, M., Zimmermann, S.: Improving Ion Mobility Spectrometer Sensitivity through the Extended Field Switching Ion Shutter. Anal. Chem. (2020). https://doi.org/10.1021/acs.analchem.9b04259
- 36. Kirk, A.T., Grube, D., Kobelt, T., Wendt, C., Zimmermann, S.: High-Resolution High Kinetic Energy Ion Mobility Spectrometer Based on a Low-Discrimination Tristate Ion Shutter, http://dx.doi.org/10.1021/acs.analchem.7b04586, (2018)
- 37. Kwantwi-Barima, P., Reinecke, T., Clowers, B.H.: Increased ion throughput using tristate ion-gate multiplexing. Analyst. 144, 6660–6670 (2019)
- 38. Xu, J., Whitten, W.B., Ramsey, J.M.: Pulsed-ionization miniature ion mobility spectrometer. Anal. Chem. 75, 4206–4210 (2003)
- 39. Cochems, P., Kirk, A.T., Bunert, E., Runge, M., Goncalves, P., Zimmermann, S.: Fast pulsed operation of a small non-radioactive electron source with continuous emission current control. Rev. Sci. Instrum. 86, 065102 (2015)
- 40. Bunert, E., Heptner, A., Reinecke, T., Kirk, A.T., Zimmermann, S.: Shutterless ion mobility spectrometer with fast pulsed electron source. Rev. Sci. Instrum. 88, 024102 (2017)
- 41. Gendreau, K., Arzoumanian, Z., Asami, F., Baker, R., Balsamo, E., Black, K., Duran-Aviles, C., Enoto, T., Gregory, K., Hahne, D., Hayato, A., Hill, J., Huegel, F., Iwahashi, T., Iwakiri, W., Jahoda, K., Jalota, L., Kaaret, P., Kaneko, K., Kenyon, S., Kitaguchi, T., Koenecke, R., Kohmura, T., Okajima, T., Olsen, L., Scott Porter, F., Rush, K., Serlemitsos, P., Soong, Y., Takeuchi, Y., Tamagawa, T., Yamada, S. 'ya, Yoshikawa, A.: The x-ray advanced concepts testbed (XACT) sounding rocket payload. In: Space Telescopes and Instrumentation 2012: Ultraviolet to Gamma Ray. p. 84434V. International Society for Optics and Photonics (2012)
- 42. Reinecke, T., Clowers, B.H.: Implementation of a flexible, open-source platform for ion mobility spectrometry. HardwareX. 4, e00030 (2018)
- 43. Bohnhorst, A., Kirk, A.T., Zimmermann, S.: Simulation aided design of a low cost ion mobility spectrometer based on printed circuit boards, http://dx.doi.org/10.1007/s12127-016-0202-7, (2016)
- 44. Gendreau, K.C., Arzoumanian, Z., Kenyon, S.J., Spartana, N.S.: Miniaturized high-speed modulated X-ray source, https://patentimages.storage.googleapis.com/93/75/8c/c73f4dc48679b3/US9117622.p df, (2015)
- 45. Harwit, M., Sloane, N.J.A.: Hadamard Transform Optics. Academic Press (1979)
- 46. Clowers, B.H., Belov, M.E., Prior, D.C., Danielson, W.F., 3rd, Ibrahim, Y., Smith, R.D.:

- Pseudorandom sequence modifications for ion mobility orthogonal time-of-flight mass spectrometry. Anal. Chem. 80, 2464–2473 (2008)
- 47. Kumbhani, S.R., Wingen, L.M., Perraud, V., Finlayson-Pitts, B.J.: A cautionary note on the effects of laboratory air contaminants on ambient ionization mass spectrometry measurements. Rapid Commun. Mass Spectrom. 31, 1659–1668 (2017)
- 48. Watts, P.: Studies on gas-phase negative ion/molecule reactions of relevance to ion mobility spectrometry: kinetic modelling of the reactions occurring in "clean" air. Int. J. Mass Spectrom. Ion Process. 121, 141–158 (1992)
- 49. Waltman, M.J., Dwivedi, P., Hill, H.H., Jr, Blanchard, W.C., Ewing, R.G.: Characterization of a distributed plasma ionization source (DPIS) for ion mobility spectrometry and mass spectrometry. Talanta. 77, 249–255 (2008)
- 50. Sekimoto, K., Sakai, M., Takayama, M.: Specific interaction between negative atmospheric ions and organic compounds in atmospheric pressure corona discharge ionization mass spectrometry. J. Am. Soc. Mass Spectrom. 23, 1109–1119 (2012)
- 51. Trötzmüller, M., Guo, X., Fauland, A., Köfeler, H., Lankmayr, E.: Characteristics and origins of common chemical noise ions in negative ESI LC-MS. J. Mass Spectrom. 46, 553–560 (2011)
- 52. Siems, W.F., Wu, C., Tarver, E.E., Hill, H.H., Jr., Larsen, P.R., McMinn, D.G.: Measuring the Resolving Power of Ion Mobility Spectrometers. Anal. Chem. 66, 4195–4201 (1994)
- 53. Grabarics, M., Lettow, M., Kirk, A.T., von Helden, G., Causon, T.J., Pagel, K.: Plateheight model of ion mobility-mass spectrometry. Analyst. 145, 6313–6333 (2020)
- 54. Vautz, W., Bödeker, B., Baumbach, J.I., Bader, S., Westhoff, M., Perl, T.: An implementable approach to obtain reproducible reduced ion mobility. Int. J. Ion Mobil. Spectrom. 12, 47–57 (2009)
- 55. Spangler, G.E.: Theory and technique for measuring mobility using ion mobility spectrometry. Anal. Chem. 65, 3010–3014 (1993)
- 56. Nitzsche, G., Riesenberg, R.: Noise, fluctuation, and HADAMARD-transform spectrometry. In: Fluctuations and Noise in Photonics and Quantum Optics. pp. 273–283. International Society for Optics and Photonics (2003)
- 57. Reinecke, T., Naylor, C.N., Clowers, B.H.: Ion multiplexing: Maximizing throughput and signal to noise ratio for ion mobility spectrometry. Trends Analyt. Chem. 116, 340–345 (2019)
- 58. Hong, Y., Huang, C., Liu, S., Xia, L., Shen, C., Chu, Y.: Normal-inverse bimodule operation Hadamard transform ion mobility spectrometry. Anal. Chim. Acta. 1029, 44–49 (2018)
- 59. Hong, Y., Niu, W., Gao, H., Xia, L., Huang, C., Shen, C., Jiang, H., Chu, Y.: Rapid identification of false peaks in the spectrum of Hadamard transform ion mobility spectrometry with inverse gating technique. RSC Adv. 5, 56103–56109 (2015)